Materials Today Bio 29 (2024) 101340

Contents lists available at ScienceDirect

Materials Today Bio

journal homepage: www.journals.elsevier.com/materials-today-bio

MSCs-derived ECM functionalized hydrogel regulates macrophage reprogramming for osteoarthritis treatment by improving mitochondrial function and energy metabolism

Zhuolin Chen [a,b,c,1], Qiming Pang [a,b,c,1], Jingdi Zhan [a,b,c], Junyan Liu [a,b,c], Weikang Zhao [a,b,c,***], Lili Dong [a,b,c,**], Wei Huang [a,b,c,*]

[a] Department of Orthopaedic Surgery, The First Affiliated Hospital of Chongqing Medical University, Chongqing, China
[b] Chongqing Municipal Health Commission Key Laboratory of Musculoskeletal Regeneration and Translational Medicine, The First Affiliated Hospital of Chongqing Medical University, Chongqing, China
[c] Orthopaedic Research Laboratory of Chongqing Medical University, Chongqing Medical University, Chongqing, China

ARTICLE INFO

Keywords:
Osteoarthritis
Mesenchymal stem cells
Extracellular matrix
Macrophage polarization
Mitochondria

ABSTRACT

Osteoarthritis (OA) is a degenerative disease that affects the entire joint, with synovial inflammation being a major pathological feature. Macrophages, as the most abundant immune cells in the synovium, have an M1/M2 imbalance that is closely related to the occurrence and development of OA. Mesenchymal stem cells (MSCs) have been shown to effectively suppress inflammation in the treatment of OA, but they still pose issues such as immune rejection and tumorigenicity. The extracellular matrix (ECM), as a major mediator of MSCs' immunoregulatory effects, offers a cell-free therapy to circumvent these risks. In this study, we developed an ECM-functionalized hydrogel by combining MSC-derived ECM with gelatin methacryloyl (GelMA). To enhance the immunomodulatory potential of MSCs, we pre-stimulated MSCs with the inflammatory factor interleukin-6 (IL-6) present in OA. In vitro results showed that the ECM-functionalized hydrogel promoted M2 macrophage polarization and inhibited the expression of various inflammatory genes, strongly indicating the hydrogel's powerful immunoregulatory capabilities. In an in vivo rat OA model, the ECM-functionalized hydrogel significantly reduced synovial inflammation and cartilage matrix degradation, alleviating the progression of OA. Furthermore, we utilized proteomics and transcriptomics analysis to reveal that the hydrogel accomplished macrophage metabolic reprogramming by regulating mitochondrial function and energy metabolism, thereby reducing inflammation. These findings suggest that the ECM-functionalized hydrogel is a promising biomaterial-based strategy for treating OA by targeting key pathological mechanisms.

1. Introduction

Osteoarthritis (OA) is a degenerative disease that affects the entire joint, with destruction of articular cartilage and synovial inflammation being its main pathological features [1,2]. In recent years, increasing evidence has indicated that synovial inflammation is a key factor in the exacerbation of OA [3]. Macrophages, as the primary immune cells in the synovium, play a significant role in the development of OA [4]. Macrophages are typically divided into two subtypes: the classically activated M1 type and the alternatively activated M2 type [5]. M1 macrophages dominate in the early stages of inflammation by secreting pro-inflammatory cytokines such as IL-6, while M2 macrophages secrete anti-inflammatory cytokines such as IL-4 [6,7]. Studies have shown that the imbalance between M1 and M2 macrophages is positively correlated with the severity of OA, making the reprogramming of M1 macrophages into M2 macrophages crucial for treating synovial inflammation in OA patients [8,9].

Mesenchymal stem cells (MSCs) are a type of pluripotent stem cell

* Corresponding author. Department of Orthopaedic Surgery, The First Affiliated Hospital of Chongqing Medical University, Chongqing, China.
** Corresponding author. Department of Orthopaedic Surgery, The First Affiliated Hospital of Chongqing Medical University, Chongqing, China.
*** Corresponding author. Department of Orthopaedic Surgery, The First Affiliated Hospital of Chongqing Medical University, Chongqing, China.
E-mail addresses: 81329647@qq.com (W. Zhao), dllbme@alu.cqu.edu.cn (L. Dong), huangwei123@163.com (W. Huang).
[1] The authors contributed equally to this work.

https://doi.org/10.1016/j.mtbio.2024.101340
Received 10 August 2024; Received in revised form 20 October 2024; Accepted 10 November 2024
Available online 18 November 2024

with anti-inflammatory, anti-aging, and tissue regeneration properties, capable of effectively regulating macrophage reprogramming, and thus hold great promise for the treatment of OA [10–12]. However, challenges such as tumorigenicity, immune rejection, and donor heterogeneity pose significant obstacles to the clinical application of MSCs [13,14]. Therefore, the focus of research has been on maximizing the therapeutic effects of MSCs while avoiding their drawbacks. In recent years, more studies have found that the primary mechanism by which MSCs exert their functions is not through direct differentiation and tissue replacement but through paracrine pathways [15,16]. The extracellular matrix (ECM) is considered the main mediator through which MSCs promote tissue regeneration and immunoregulation. These non-cellular components not only eliminate cellular components that might cause immunogenicity in vivo but also preserve a large number of active proteins and growth factors [17–19]. Recent studies have also confirmed that decellularized ECM (dECM) can effectively regulate macrophage polarization and reprogramming to reduce inflammation, successfully applied in various fields such as bone defects, skin injuries, and tendon adhesions [20–22]. Compared to tissue-derived dECM (t-dECM), cell-derived dECM (c-dECM) not only possesses excellent

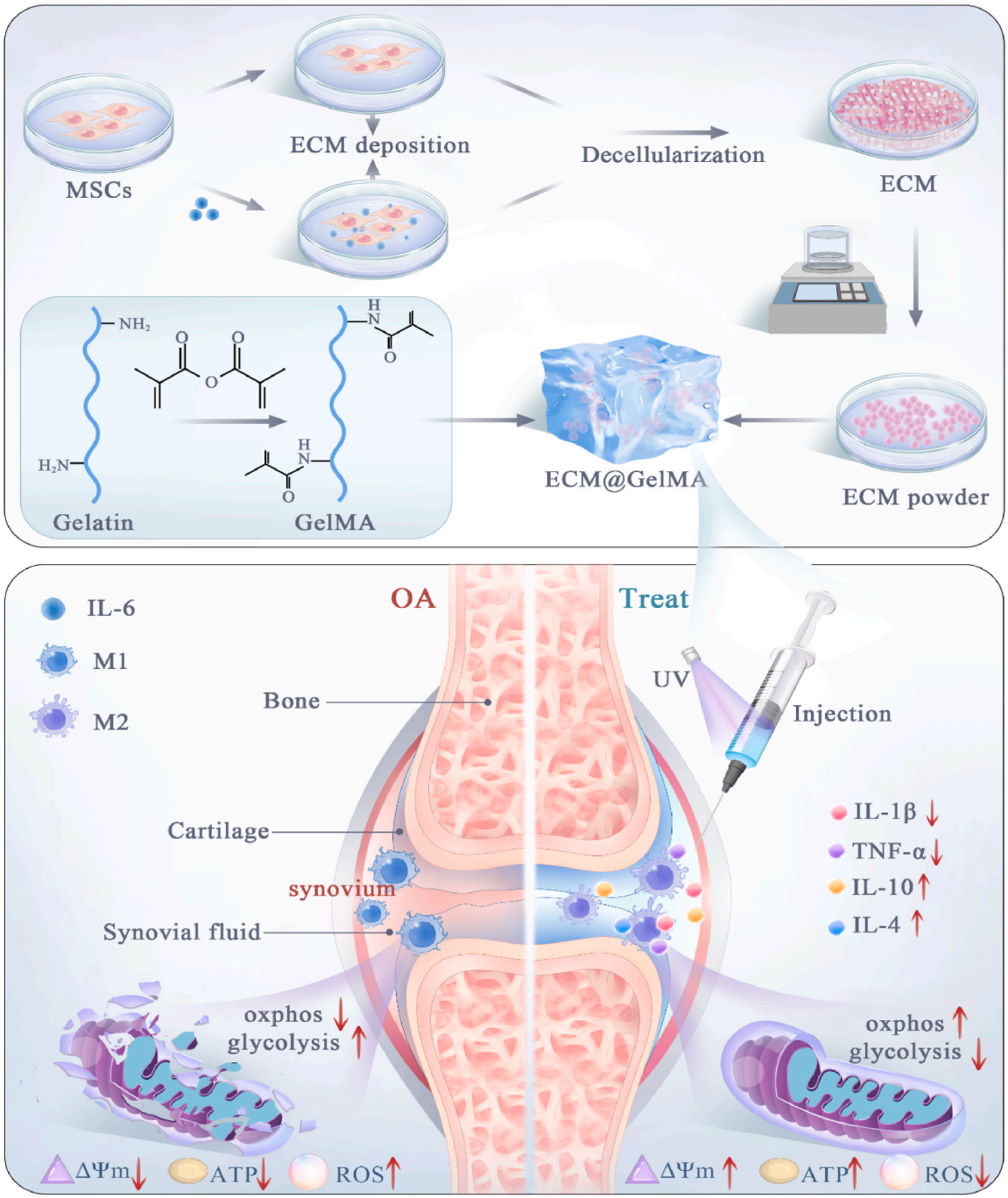

Fig. 1. Manufacture and Principle of Hydrogel:IL-6-ECM/ECM is obtained through different interventions and is processed by cryogenic grinding after lyophilization. GelMA hydrogel serves as a carrier for IL-6-ECM/ECM. When injected into the joint cavity, it can significantly inhibit M1 macrophage inflammation and promote M2 macrophage generation. This effectively restores mitochondrial dysfunction in macrophages and promotes the metabolic shift in macrophage mitochondria from glycolysis to oxidative phosphorylation.

biocompatibility but also has a wide range of sources and can even use autologous cells as the source of dECM, significantly reducing the risk of disease transmission [23–25]. Therefore, MSCs-ECM has the potential to reduce pathogen transmission and regulate macrophage reprogramming, making it an emerging strategy for treating OA.

Although MSCs-ECM has shown significant therapeutic potential, the efficacy remains limited when MSCs are cultured under traditional conditions [26,27]. Recent studies have demonstrated that MSCs are environment-responsive; their paracrine components change with different physicochemical and biological pre-stimulations. This means that exposure to the microenvironment of diseases and tissue damage can further optimize the effective components of their ECM, providing a theoretical basis for constructing better dECM [28–30]. Dong et al. demonstrated that stimulating MSCs with interferon-γ (IFN-γ), a key inflammatory factor in tendon adhesion, can significantly regulate macrophage reprogramming efficiency to reduce tendon adhesion [20]. Interleukin-6 (IL-6), an inflammatory mediator secreted by M1 macrophages, can activate destructive metabolic pathways in chondrocytes and synovial cells, promoting the expression of matrix metalloproteinases (MMPs) and ADAMTS, leading to cartilage matrix degradation [31–33]. Therefore, the high expression levels of IL-6 in OA synovial fluid are closely associated with synovial inflammation, cartilage degradation, and joint pain, making it a key inflammatory factor in synovium-cartilage crosstalk. Hence, we chose IL-6 as the "trigger" for MSCs to pre-stimulate them, thereby obtaining dECM with enhanced inflammation-regulating properties.

However, the dECM obtained through pre-stimulation has poor injectability and is easily affected by various factors in the complex in vivo environment, leading to rapid degradation and uncontrolled release, which limits its use [34]. Hydrogels are network structures composed of polymer materials that can serve as protective barriers for active proteins and growth factors, preventing damage under physiological conditions [35]. Therefore, this study lyophilized dECM and prepared it into an active powder, using gelatin, commonly found in ECM, as the basic structural material and introducing methacryloyl modification. By uniformly mixing GelMA with dECM and then photocuring it, we prepared an inflammation-regulating properties hydrogel. This experiment evaluated the effects and differences of ECM@GelMA and IL-6-ECM@GelMA in regulating synovial macrophage polarization and improving inflammation. Multi-omics studies confirmed that IL-6-ECM@GelMA might regulate macrophage reprogramming by improving mitochondrial function and energy metabolism, thereby alleviating OA. The IL-6-ECM@GelMA constructed in this study fully utilizes the biological functions of dECM. This type of natural hydrogel, with good biocompatibility and anti-inflammatory properties, provides a new strategy for both dECM research and OA treatment (see Fig. 1).

2. Materials and methods

2.1. Preparation and characterization of ECM

ECM was prepared following previously reported methods [36]. We used C3H/10T1/2 as the MSCs model cell line for subsequent experiments. Briefly, MSCs were seeded at a density of 5 × 10^5 cells per well in TCP culture plates. The cells were cultured in DMEM (Beyotime, China) medium supplemented with 10 % fetal bovine serum (FBS) (Beyotime, China) and 1 % penicillin/streptomycin (Life Technologies, Beyotime, China). The medium was changed three times a week, and to activate the ECM's immunoregulatory abilities, IL-6 (20 ng/ml) (MCE, USA) was added to the DMEM medium. After 14 days of culture, the decellularization process was carried out using a physical and chemical approach. In brief, the ECM was frozen at −80 °C for 2 h, thawed at room temperature, and then washed with Milli-Q water to remove cell debris. This process was repeated three times, followed by treatment with 20 mM ammonium hydroxide for 15 min, and then washed with Milli-Q water. Finally, optical microscopy was used to confirm the removal of cellular material, resulting in the preparation of ECM and IL-6-ECM.

To assess the effectiveness of decellularization and the retention of bioactive components, we used both immunofluorescence and scanning electron microscopy (SEM). First, Hoechst 33342 live cell staining reagent (Beyotime, China) and FITC-labeled phalloidin (Solarbio, China) were used to stain the cell nuclei and cytoskeleton, respectively. Unprocessed MSCs-ECM was used as a control and was similarly treated and observed under a fluorescence microscope.

Next, samples were fixed, blocked, and incubated overnight with primary antibody against fibronectin (Proteintech, China), followed by 1 h of incubation at room temperature with corresponding rabbit secondary antibody, and then stained with DAPI (Beyotime, China). Fluorescence microscopy was used to observe and capture images.

Field emission scanning electron microscopy (SEM) was used to observe the microscopic morphology of ECM. Samples were fixed with glutaraldehyde, subjected to a gradient ethanol dehydration process, and then critical point dried with carbon dioxide. After sputtering with gold, samples were examined and photographed using a field emission scanning electron microscope (Hitachi, Japan).

2.2. Effect of ECM on macrophage polarization

To investigate the effect of ECM on macrophage polarization, we cultured macrophages in 24-well plates with ECM or IL-6-ECM, and stimulated them with 200 ng/ml LPS the following day to induce M1 macrophages. After 3 days, the culture was terminated and the macrophages were subjected to immunofluorescence staining for CD86 (Proteintech, China) and CD206 (Proteintech, China). In brief, the cells were first fixed with 4 % paraformaldehyde for 30 min, then permeabilized with Triton X-100 (0.1 %) for 5 min, and blocked with 1 % BSA for 1 h. The primary antibodies for CD86 (1:200) and CD206 (1:200) were added and incubated overnight at 4 °C. Afterward, the secondary antibodies, CoraLite®594 (1:500) (Proteintech, China) and CoraLite®488 (1:500) (Proteintech, China), were incubated at 37 °C for 1 h. The cell nuclei were stained with DAPI staining reagent (Beyotime, China). The samples were observed and imaged using a confocal laser scanning microscope (Nikon, Japan).

2.3. Preparation and Characterization of ECM functionalized hydrogel

To prepare the ECM@GelMA hydrogels, lyophilized GelMA (40 mg) (EFL-GM-60, China) was dissolved in 1 ml of PBS containing lithium acylphosphinate (LAP) salt (0.2 % w/v). The GelMA solution was then filtered through a 0.22 μm membrane. Subsequently, the ECM was freeze-dried and ground into ECM powder in a liquid nitrogen environment. The ECM powder was added to the GelMA solution and stirred overnight in the dark to obtain ECM@GelMA. The microscopic morphology of ECM@GelMA was observed using field emission scanning electron microscopy (SEM). Additionally, to assess the ECM distribution within the hydrogel, the cross-linked hydrogels were fixed, blocked, and incubated overnight with a primary antibody against fibronectin (Proteintech, China), followed by a 1-h incubation with a corresponding secondary antibody at room temperature, and the distribution was observed and imaged using confocal laser scanning microscopy.

To further evaluate the properties of ECM@GelMA, rheological performance tests were conducted. Briefly, the cross-linked hydrogels were placed on the sample stage, and the strain-modulus of the hydrogel was tested at a frequency of 1 Hz at temperatures of 25 °C and 4–40 °C using a rotational rheometer (Anton Paar, Austria). Additionally, the shear rate of the hydrogel was tested from 0.1 to 1000 s-1.

To evaluate the degradation performance of ECM@GelMA, the cross-linked hydrogels were placed in wells, and PBS and collagenase type II (2.5 U/ml) were added to simulate the in vivo microenvironment. The initial weight (M0) was recorded, and to maintain enzyme activity, the type II collagenase solution was replaced every 2 days. At predetermined

times, the weight of the hydrogel (Md) was measured. The degradation percentage was calculated using the formula: Mt = (M0 − Md)/M0 × 100 %.

2.4. Biocompatibility evaluation of the ECM functionalized hydrogel

To evaluate the biocompatibility of the hydrogels, live/dead staining and CCK-8 assays were performed. Briefly, GelMA, ECM@GelMA, and IL-6-ECM@GelMA were injected into confocal dishes and UV-cured for 30 s. Macrophages were then seeded onto the dishes. On days 1, 2, and 3, the safety of the hydrogels was assessed using a Calcein/PI cell viability and cytotoxicity assay kit (Beyotime, China), and observations were made using a confocal laser scanning microscope. Additionally, at the same time points, 10 % CCK-8 (MCE, USA) reagent was added to the culture medium and incubated for 1 h. The optical density (OD) of the medium at 450 nm was measured using a microplate reader.

2.5. Effects of ECM functionalized hydrogel on macrophage polarization

To study the effects of the hydrogels on macrophage polarization, macrophages were seeded onto GelMA hydrogels and GelMA hydrogels containing ECM and IL-6-ECM, respectively. The following day, the macrophages were stimulated with 200 ng/ml LPS to induce M1 macrophage polarization. After 48 h of incubation with ECM hydrogels and treated macrophages, immunofluorescence staining was performed to analyze macrophage polarization levels using CD86 (M1 marker) and CD206 (M2 marker). Briefly, the cells were fixed with 4 % paraformaldehyde for 30 min, permeabilized with Triton X-100 (0.1 %) for 5 min, and then blocked with 1 % BSA for 1 h. CD86 (1:200) and CD206 (1:200) primary antibodies were added and incubated at 4 °C overnight. After that, secondary antibodies CoraLite®594 (1:500) and CoraLite®488 (1:500) were added and incubated at 37 °C for 1 h. The cells were stained with DAPI (Beyotime, China) to visualize the nuclei. The staining was observed and photographed using a confocal laser scanning microscope.

Total RNA was extracted from the macrophages using an RNA extraction kit (Accurate Biology, China). The RNA was then reverse transcribed into cDNA using a reverse transcription kit (RT Master Mix for qPCR) (MCE, China). The mRNA expression levels were detected using a CFX96 real-time PCR detection system (Bio-Rad, USA). The primer sequences for CD86, IL-1β, CD206, ARG-1, and GAPDH are listed in Table S1.

Cytokine levels for IL-6 (Thermo Fisher Scientific, USA), TNF-α (Thermo Fisher Scientific, USA), IL-4 (Thermo Fisher Scientific, USA), and IL-10 (Thermo Fisher Scientific, USA) were measured using ELISA kits according to the manufacturer's instructions. Briefly, the treated macrophages were added to the ELISA plates provided by the kits. After 90 min of incubation at 37 °C, biotin-conjugated antibody solution, avidin-HRP solution, TMB substrate solution, and stop solution were sequentially added to each well. The optical density at 450 nm was measured within 15 min.

2.6. Effects of reprogrammed macrophages on chondrocytes

To investigate the effects of reprogrammed macrophages on chondrocytes, chondrocytes were stimulated with 20 ng/ml IL-1β for 1 day. The supernatants from macrophages treated with Blank, ECM@GelMA, and IL-6-ECM@GelMA were then added to the chondrocytes, and immunofluorescence staining for MMP13 was performed. Briefly, the cells were fixed with 4 % paraformaldehyde for 30 min, permeabilized with Triton X-100 (0.3 %) for 15 min, and then blocked with 1 % BSA for 1 h. MMP13 (Proteintech, China) primary antibody (1:200) was added and incubated at 4 °C overnight. The cells were then incubated with CoraLite®594 (1:500) at 37 °C for 1 h. The nuclei were stained with DAPI (Beyotime, China). The staining was observed and photographed using a confocal laser scanning microscope.

2.7. Proteomics

To analyze the protein composition of the extracellular matrix (ECM), protein extracts from different intervention groups (ECM, IL-6-ECM) were collected, with three replicates per group. The protein concentration of each group was determined using the BCA Protein Assay Kit, and then the proteins were separated by SDS-PAGE. After electrophoresis, the gel was photographed. For protein digestion, trypsin was added to the samples, which were then incubated and desalinated. TMT labeling was used to tag the peptides with specific labels. Peptides were fractionated using reversed-phase high-performance liquid chromatography (HPLC), collected into fractions, and then lyophilized. Quantitative analysis was performed by Nano-LC-MS/MS, where peptides were separated and analyzed using a mass spectrometer. Equal amounts of peptides from all samples were mixed, diluted with mobile phase A (5 % ACN, pH 9.8), and injected for separation using the UltiMate™ 3000 Binary Rapid Separation System (Thermo Scientific, USA). Peptides were collected at a wavelength of 214 nm and then lyophilized. The peptides were then separated using the EASY-nLC™ 1200 System (Thermo Scientific, USA), and the separated peptides were ionized using a nanoESI source and analyzed by mass spectrometry with the Orbitrap Exploris™ 480 (Thermo Fisher Scientific, San Jose, CA) in Data-Dependent Acquisition (DDA) mode. Finally, MaxQuant software was used for protein identification and quantification, with strict criteria applied to ensure accuracy. The Uniprot database for the corresponding species was used as the default database, with a spectral FDR and protein FDR set at 1 % for protein filtering.

2.8. RNA-seq

Total RNA was isolated and purified from macrophages treated with GelMA and IL-6-ECM@GelMA using TRIzol (Thermo Fisher, USA). The RNA samples were then subjected to paired-end sequencing (PE150) using the Illumina NovaseqTM 6000 (LC Bio Technology CO., Ltd., Hangzhou, China) according to standard procedures. The sequencing data were filtered to obtain high-quality sequencing data (Clean Data), and then analyzed using the R programming language. Differentially expressed genes (DEGs) with a fold change $\geq$2 and a p-value $\leq$0.05 were identified. The identified DEGs were subjected to functional annotation in Gene Ontology (GO) and gene set enrichment analysis (GSEA).

2.9. Mitochondrial transmission electron microscopy

The treated macrophages were fixed in 2.5 % glutaraldehyde at 4 °C overnight. The cells were then washed and fixed in 1 % osmium tetroxide for 1 h. Following fixation, the specimens were dehydrated using an ethanol gradient, embedded in resin, and sectioned into ultrathin slices. The sections were stained with uranyl acetate and lead citrate. Mitochondria in the cells were observed using Transmission Electron Microscopy (TEM, Hitachi, Japan).

2.10. Mitochondrial function

The mitochondrial membrane potential (ΔΨm) of macrophages was measured using the Enhanced Mitochondrial Membrane Potential Assay Kit with JC-1 (Beyotime, China). Briefly, after 48 h of treatment, cells were washed twice with PBS and then stained with JC-1 at 37 °C for 20 min. After staining, the cells were washed twice with JC-1 Buffer and then 1 ml of cell culture medium was added. The cells were observed using a confocal laser microscope. The ΔΨm was calculated using the ratio of red to green fluorescence intensity with ImageJ software.

ROS generation in macrophages was assessed using the ROS Detection Assay Kit (Beyotime, China). Briefly, after 48 h of treatment, cells were washed twice with PBS and then incubated with 10 μM DCFH-DA at 37 °C for 20 min. After incubation, the cells were washed with serum-free cell culture medium and then stained with Hoechst 33342 live cell

staining reagent (Beyotime, China) for nuclear staining. ROS levels were observed using a confocal laser microscope, and fluorescence intensity was measured using ImageJ software.

ATP production in macrophages was measured using the Enhanced ATP Assay Kit (Beyotime, China). After 48 h of treatment, cells were washed twice with PBS and then lysed with 200 μL/well of lysis buffer. The lysates were centrifuged at 12,000 g at 4 °C, and the supernatant was transferred to a 96-well plate containing ATP working solution. ATP production was measured using a fluorescence spectrophotometer.

2.11. Osteoarthritis Rat Model

This study was approved by the Institutional Animal Care and Use Committee (IACUC) of Chongqing Medical University. To evaluate the therapeutic effect of IL-6-ECM@GelMA, we established an OA model in 12-week-old male Sprague-Dawley (SD) rats using the medial meniscus transection (DMM) surgical procedure. Three days post-surgery, antibiotics (penicillin, 100,000 units administered intramuscularly daily) and analgesics (carprofen, 1 mg per rat daily in gel form) were administered to prevent postoperative infection and to avoid animals licking the wound. Three weeks later, OA rats were randomly divided into 3 groups, with 5 rats per group, and treated with PBS, ECM@GelMA, or IL-6-ECM@GelMA via intra-articular injection. All animal experiments were conducted under sterile conditions.

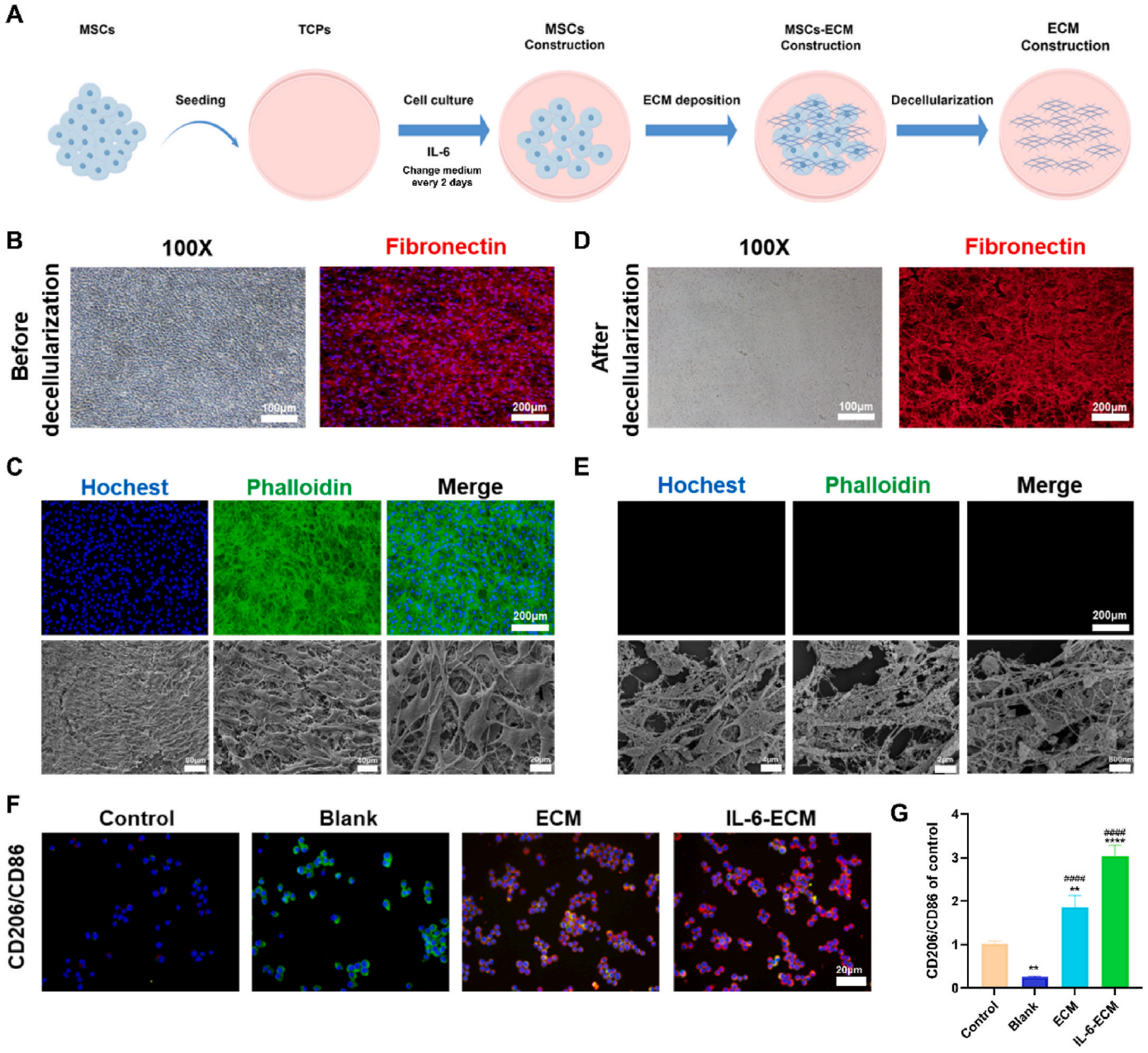

Fig. 2. Extraction and Characterization of ECM. A. ECM is obtained through different intervention methods and decellularization. B. Light microscopy image and fibronectin fluorescence image before decellularization. C. Staining of cell nuclei and cytoskeleton before decellularization. D. Light microscopy image and fibronectin fluorescence image after decellularization. E. Staining of cell nuclei and cytoskeleton after decellularization. F. Representative immunofluorescence images of macrophages cultured on ECM and IL-6-ECM, showing CD86 (M1 marker, green), CD206 (M2 marker, red), and DAPI (Nuclei, blue). (Data are expressed as mean ± standard deviation, n = 3, */**/***/**** and#/##/###/#### indicated $p < 0.05/p < 0.01/p < 0.001/p < 0.0001$ in comparison with the Control and Blank groups, respectively).

2.12. Histological examination

Eight weeks after the establishment of the OA model, the animals were euthanized, and the knee joints were collected and fixed in 4 % paraformaldehyde. The knee joints were then decalcified, embedded, and sectioned in the sagittal plane. Histological analysis was performed on the sections using Hematoxylin and Eosin (H&E) staining and Safranin-O Fast Green staining. Immunofluorescence antibodies used included MMP13 (Proteintech, China), CD206 (Proteintech, China), and CD86 (Proteintech, China). After overnight incubation at 4 °C with the primary antibodies, sections were incubated with Cy3 Tyramide (Servicebio, China) at 4 °C for 30 min, followed by DAPI staining for 10 min. Imaging was performed using a fluorescence microscope. The expression levels of MMP13, CD86, and CD206 were quantified using ImageJ software.

2.13. Statistical analysis

In vitro experiments were performed in triplicate, while in vivo experiments were conducted in quintuplicate. Data were analyzed using GraphPad Prism (9.0), and results are presented as mean ± standard deviation. Statistical comparisons were made using Student's t-test (for two groups) or one-way/two-way ANOVA (for multiple groups), followed by Tukey-Kramer post-hoc test. A p-value of <0.05 was considered to indicate statistical significance.

3. Result and discussion

3.1. Characterization of ECM

First, MSCs were cultured under two conditions: normal complete medium and IL-6 pre-stimulation conditions. After continuous culture for 14 days, the MSCs were removed using freeze-thaw washing and ammonia treatment to obtain ECM and IL-6-ECM, respectively (Fig. 2A). Residual cell nuclei and cytoskeletons are the main sources of antigenic reactions, and both optical microscopy and fluorescence microscopy after DAPI staining confirmed that the cell nuclei were removed before and after decellularization. Fluorescence staining showed that fibronectin, a major component of ECM, was well preserved (Fig. 2B and C). To further confirm the effectiveness of decellularization, we used Hoechst and FITC-conjugated phalloidin staining to label cells. The results showed that compared to before decellularization, neither of the fluorescent stains was observed under the microscope after decellularization, indicating that the freeze-thaw and ammonia treatment method was effective. Additionally, scanning electron microscopy (SEM) showed no remaining cellular structures after decellularization and revealed the typical fibrous structure of ECM (Fig. 2D and E). These results confirm that we successfully extracted two types of ECM.

3.2. The effect of ECM on macrophage polarization

To evaluate the effects of the two ECMs on macrophage polarization, macrophages were subjected to different treatments. Since CD206 and CD86 are markers for M2 and M1 macrophages, respectively, we analyzed macrophage phenotypes through immunofluorescence staining and the CD206/CD86 fluorescence intensity ratio. In the experiment, the control group received no treatment, while the Blank group was stimulated with 200 ng/ml LPS. Fluorescence intensity analysis showed a significant decrease in the CD206/CD86 ratio, indicating a shift of macrophages towards the M1 phenotype. However, the addition of both ECMs along with LPS resulted in the suppression of M1 polarization and promoted M2 macrophage polarization, with IL-6-ECM exhibiting a stronger regulatory effect ($P < 0.05$) (Fig. 2F and G).

3.3. ECM functionalized hydrogel characterization

The poor injectability of ECM and its high clearance rate within the joint cavity are significant challenges for its use. To address these issues, we freeze-dried the ECM and ground it into a powder under liquid nitrogen, then thoroughly mixed it with GelMA to obtain ECM@GelMA hydrogel through photopolymerization (Fig. 3A). To verify the successful incorporation of ECM into the hydrogel, we used immunofluorescence to label fibronectin with red fluorescence and performed 3D layer scanning with confocal microscopy. Both cross-sectional images and 3D reconstructions showed a uniform distribution of red fluorescence, indicating that ECM is evenly distributed within the hydrogel, which is beneficial for the uniform and sustained release of active components from ECM (Fig. 3B). To assess the injectability of the hydrogel, we injected ECM@GelMA using a 1 ml syringe and shaped it into the letter "C" without blocking the needle (Fig. 3C). This demonstrates that ECM@GelMA can be injected through minimally invasive needles into closed cavities, such as the joint cavity (Fig. 3C). Scanning Electron Microscopy (SEM) was used to characterize the microstructure of the two hydrogels, revealing a porous and loose structure after freeze-drying (Fig. 3D).

Rheology, the study of material deformation and flow, plays a crucial role in hydrogel research as a means to understand the internal structure of materials. We first tested the rheological properties of ECM@GelMA hydrogel by measuring changes in the storage modulus (G') and loss modulus (G'') with temperature variation. At 25 °C and a frequency of 1 Hz, G' was greater than G'' across a strain range of 0.1%–100 %, indicating that ECM@GelMA remains a viscoelastic gel within this strain range (Fig. 3E). Additionally, as the temperature increased from 4 °C to 40 °C, G' decreased from 423.77 Pa to 20.8 Pa, and G'' decreased from 5.09 Pa to 3.52 Pa under 1 % strain and 5 Hz frequency, demonstrating that the crosslinked 4 % GelMA + ECM hydrogel maintains its gel state across the temperature range of 4–40 °C (Fig. 3F). Furthermore, we observed that as the shear rate increased, the viscosity of ECM@GelMA decreased from 100,000 Pa s to around 1000 Pa s, exhibiting shear-thinning hydrogel behavior (Fig. 3G). The degradation rate is also an important factor affecting the functionality of ECM hydrogels. We simulated an in vivo environment by maintaining a temperature of 37 °C and adding type II collagenase to mimic the joint cavity environment. The results showed that the hydrogel degraded at a relatively uniform rate, with nearly complete degradation by day 18 (Fig. 3H).

As a biomaterial, ECM hydrogel should exhibit excellent biocompatibility. We cultured macrophages on Control, ECM@GelMA, and IL-6-ECM@GelMA groups and assessed cytotoxicity using the CCK-8 assay and Live/Dead staining. The results showed no significant differences between the two materials and the Control group at 1, 2, and 3 days of culture, indicating that both natural hydrogels have good biocompatibility ($P < 0.05$) (Fig. S1).

3.4. Effects of ECM functionalized hydrogel on macrophages

To further verify the immunoregulatory capabilities of the two hydrogels, we assessed their effects on macrophage polarization using immunofluorescence, qPCR, and ELISA. Firstly, we performed immunofluorescence staining for CD86 and CD206 and analyzed the fluorescence intensity and ratio of these markers. The experimental results showed that after LPS stimulation, the expression of CD86 in macrophages significantly increased, indicating an M1 polarization state. Both types of hydrogels were able to inhibit excessive M1 polarization while promoting the increase of M2 macrophages, with IL-6-ECM@GelMA demonstrating a stronger effect. This result is consistent with the effects of the two ECM treatments on macrophages ($P < 0.05$) (Fig. 4A–D). Furthermore, we evaluated the expression of M1 and M2 macrophage-related genes through qPCR, including CD86, IL-1β, TNF-α, CD206, and ARG-1. The results further confirmed that both hydrogels modulated macrophage polarization, with IL-6-ECM@GelMA showing a

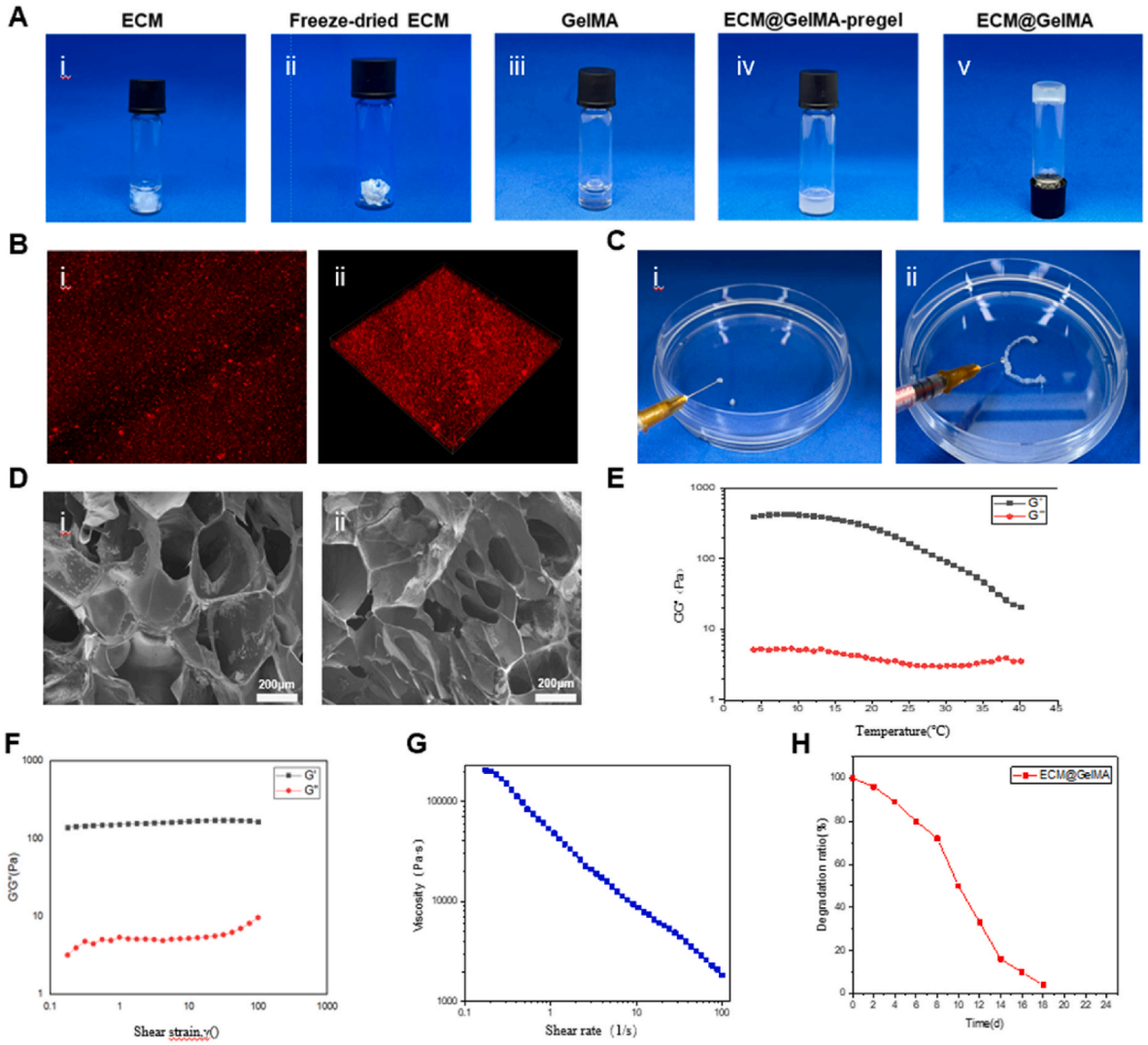

Fig. 3. Preparation and Characterization of ECM functionalized Hydrogel: A. Schematic diagram of hydrogel preparation based on ECM. B. Confocal layered (i) and z-stack scanning images (ii) of ECM@GelMA, with red fluorescence indicating fibronectin-labeled ECM. C. Injectability of the hydrogel and extrusion of hydrogel in the shape of a "C". D. Scanning electron microscopy (SEM) images of GelMA (i) and ECM@GelMA (ii) hydrogels. E. Modulus variation curve of ECM@GelMA (temperature from 4 °C to 40 °C). F. Strain modulus curve of ECM@GelMA. G. Shear rate-viscosity curve of ECM@GelMA. H. Degradation curve of ECM@GelMA over time.

stronger anti-inflammatory regulatory effect ($P < 0.05$) (Fig. 4E–H). Finally, since the regulation of macrophage polarization alone has limitations and does not fully reflect changes in the cellular microenvironment, we used ELISA to measure the levels of IL-6, TNF-α, IL-4, and IL-10 in the culture supernatant. The results showed that while the pro-inflammatory cytokines increased significantly under LPS stimulation, both ECM@GelMA and IL-6-ECM@GelMA significantly promoted the secretion of anti-inflammatory cytokines by macrophages, improving the microenvironment and inhibiting further inflammation. Additionally, IL-6-stimulated ECM@GelMA exhibited a stronger anti-inflammatory effect ($P < 0.05$) (Fig. 4I–L).

In summary, our experimental results demonstrate that ECM hydrogels not only promote the polarization of macrophages towards the M2 phenotype but also inhibit the expression of various inflammatory factors in the cells and microenvironment. Furthermore, IL-6-stimulated ECM exhibits stronger immunoregulatory capabilities.

3.5. Effects of reprogrammed macrophages on chondrocytes

Macrophage polarization dysregulation and chondrocyte homeostasis imbalance are major issues in OA, and their interactions can exacerbate the progression of OA [37]. To investigate whether reprogrammed macrophages can reduce inflammation in chondrocytes, we added the supernatant from reprogrammed macrophages to chondrocytes under a state of homeostasis imbalance and performed immunofluorescence staining to evaluate the effects. The results showed that the supernatant from M1 macrophages upregulated MMP13 expression in chondrocytes, while the supernatant from reprogrammed macrophages significantly reduced MMP13 expression, with IL-6-ECM@GelMA demonstrating a better effect ($P < 0.05$) (Fig. S2).

3.6. Overview of omics analysis of ECM

Regardless of whether ECM is directly applied or loaded onto GelMA, both approaches demonstrate significant effects in macrophage regulation and inflammatory microenvironment modulation, with IL-6-ECM exhibiting stronger capabilities. However, the specific mechanisms behind these effects remain unclear. ECM, as a paracrine complex, primarily functions through its protein components. Therefore, we conducted a proteomics analysis of the two types of ECM to further

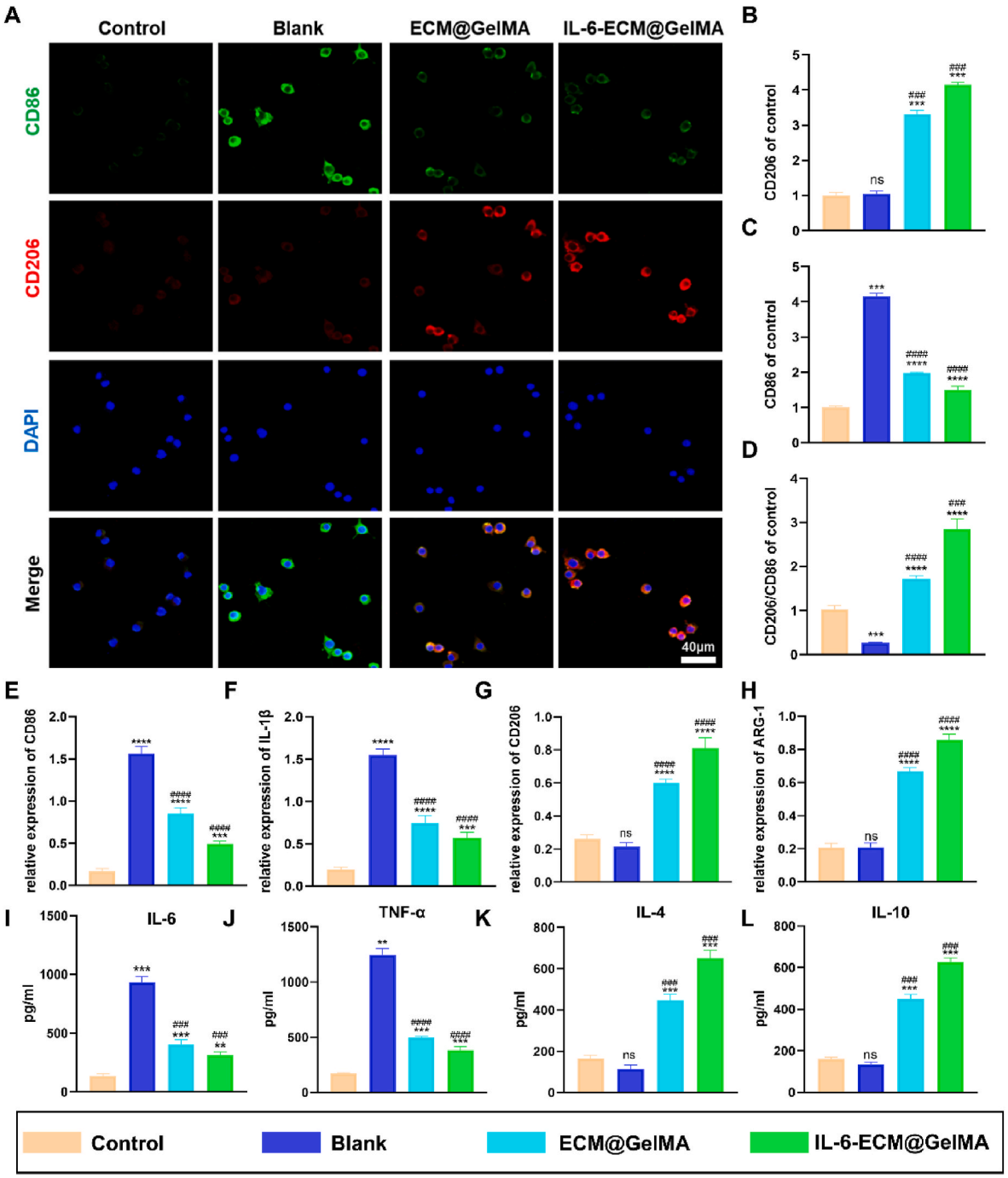

Fig. 4. Regulation of Macrophage Polarization by ECM functionalized Hydrogel In Vitro. A-B. Immunofluorescence images of RAW cells showing CD86 (M1 marker, green), CD206 (M2 marker, red), and DAPI (Nuclei, blue). E-H. Gene expression levels of CD86, IL-1β, CD206, and ARG-1 in macrophages of each group, detected by RT-PCR. I-M. ELISA detection of IL-6, TNF-α, IL-4, and IL-10 levels in the supernatant of macrophages from each group. (Data are expressed as mean ± standard deviation, n = 3, */**/***/**** and#/##/###/#### indicated $p < 0.05/p < 0.01/p < 0.001/p < 0.0001$ in comparison with the Control and Blank groups, respectively).

elucidate their potential mechanisms. The proteomics results revealed significant differences between the two ECMs. GO analysis indicated that these differential proteins are mainly enriched in pathways related to ATP synthesis, inflammatory response, extracellular matrix, and macrophage polarization regulation. KEGG analysis showed that the differential proteins are enriched in pathways associated with oxidative phosphorylation, HIF-1 signaling, and cell adhesion (Fig. 5A–C). These findings demonstrate that IL-6-induced inflammatory activation involves various signaling pathways related to immune regulation and energy metabolism. Additionally, they suggest that IL-6-ECM may achieve a metabolic reprogramming of macrophages to enhance the expression of anti-inflammatory factors.

To further elucidate the molecular mechanisms underlying macrophage reprogramming induced by the hydrogel treatment, we performed transcriptome analysis on macrophages treated with LPS and LPS + IL-6-ECM@GelMA. The results revealed 3493 differentially expressed genes between the Blank group and the IL-6-ECM@GelMA group (Fig. S3), with 1535 genes upregulated and 1958 genes downregulated. GO enrichment analysis indicated that these differential genes are primarily associated with mitochondrial function,

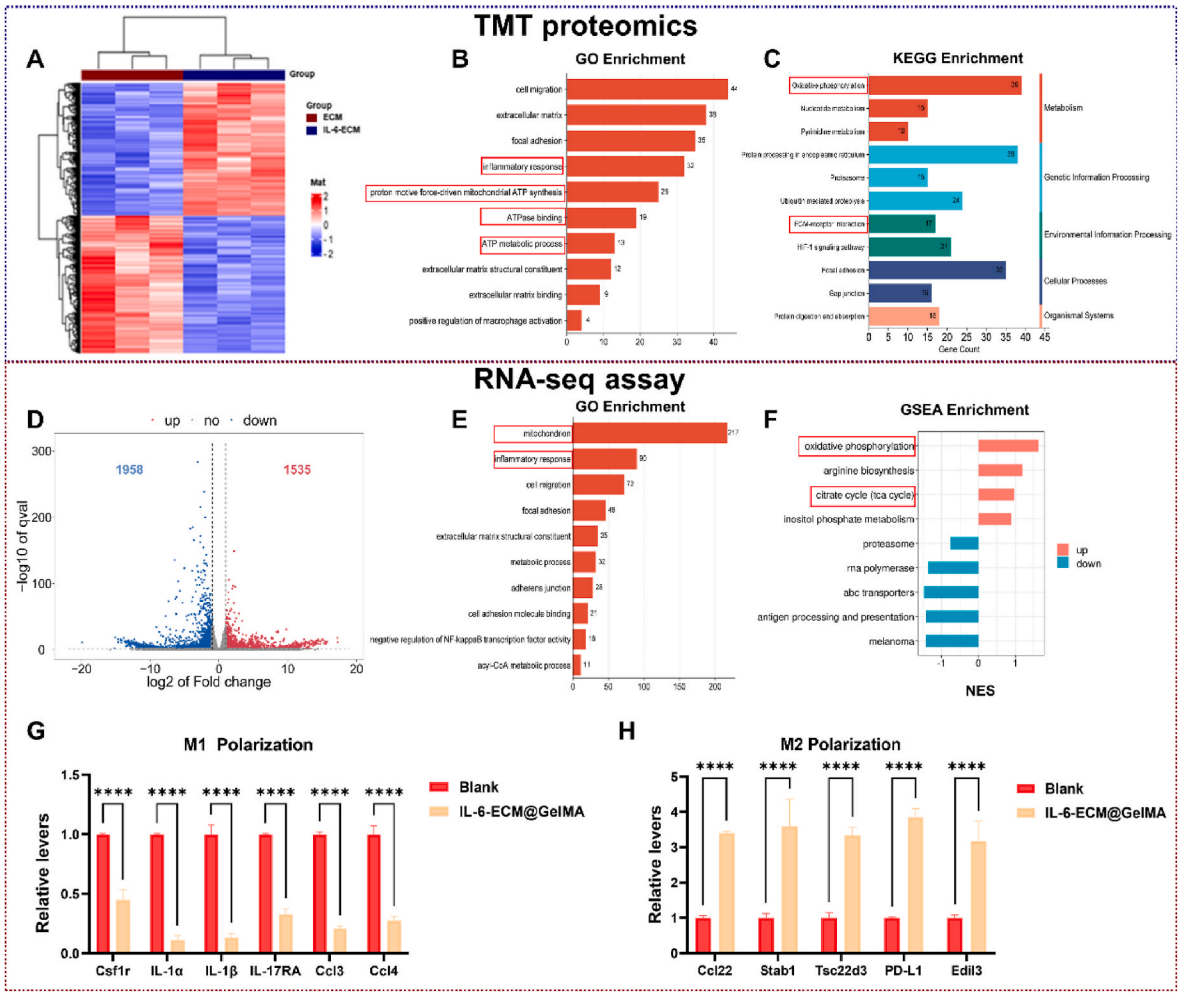

Fig. 5. Proteomics and Transcriptomics Analysis: A. Heatmap analysis of differentially expressed genes in IL-6-ECM/ECM. B. GO enrichment of differentially expressed genes in IL-6-ECM/ECM. C. KEGG enrichment of differentially expressed genes in IL-6-ECM/ECM. D. Volcano plot showing genes regulated by IL-6-ECM@GelMA treatment. E. GO enrichment of differentially expressed genes between the Blank group and the IL-6-ECM@GelMA group. F. GSEA analysis of differentially expressed genes between the Blank group and the IL-6-ECM@GelMA group. G-H. Macrophage polarization-related genes, n = 3. (Data are expressed as mean ± standard deviation, n = 3, */**/***/**** indicated $p < 0.05$/$p < 0.01$/$p < 0.001$/$p < 0.0001$ in comparison with the Blank groups, respectively).

inflammatory response, and adhesion, while GSEA enrichment analysis revealed that these genes are significantly enriched in oxidative phosphorylation pathways (Fig. 5D–F). This suggests that IL-6-ECM@GelMA promotes a higher level of oxidative phosphorylation, which implies that it regulates macrophage metabolic reprogramming by altering mitochondrial function and metabolism. Recent studies have shown that macrophage polarization is highly correlated with mitochondrial function and metabolic status, with mitochondrial dysfunction being a major cause of inflammatory dysregulation. Mitochondrial metabolic functions are the primary source of the biological responses that trigger immune reactions [6,38,39]. M1 macrophages typically rely on glycolysis for ATP production even under aerobic conditions to meet the high energy demands of pro-inflammatory responses, whereas M2 macrophages primarily depend on mitochondrial oxidative phosphorylation [40]. The transition between different macrophage polarization states involves complex metabolic reprogramming, and changes in metabolism have been shown to affect macrophage polarization [41,42]. For example, Xiao et al. found that disruption of the mitochondrial respiratory chain is a major reason for the difficulty in reprogramming pro-inflammatory macrophages, and MSCs-EVs can improve mitochondrial function to facilitate macrophage metabolic reprogramming [43]. Transcriptome analysis further confirmed that IL-6-ECM@GelMA significantly inhibits the expression of pro-inflammatory macrophage-related genes while promoting the expression of anti-inflammatory macrophage-related genes ($P < 0.05$) (Fig. 5G and H).

In summary, the two analyses collectively suggest that IL-6-ECM@GelMA may have a more pronounced effect on regulating mitochondrial function and energy metabolism, indicating that macrophages undergo metabolic reprogramming through changes in mitochondrial function and energy metabolism.

3.7. *Effects of ECM functionalized hydrogel on macrophage mitochondrial function*

Mitochondrial morphology is crucial for maintaining physiological functions, and dysfunctional mitochondria can also lead to changes in mitochondrial morphology [44]. To investigate whether mitochondrial changes occurred, we used transmission electron microscopy (TEM) to observe the mitochondrial morphology in macrophages from different treatment groups. In the control group, mitochondria displayed a clearly defined elliptical shape with well-preserved cristae, whereas in the Blank group, LPS stimulation caused significant mitochondrial swelling, cristae disruption, and “vacuolation” of the mitochondria, indicating potential mitochondrial dysfunction. In contrast, after treatment with hydrogels loaded with either ECM type, there was partial restoration of

mitochondrial morphology with minimal vacuolation (Fig. 6A and B). Mitochondrial membrane potential (JC-1) is critical for maintaining mitochondrial function and oxidative phosphorylation, as it drives ATP synthesis through the proton gradient generated by the proton flow across the ATP synthase. We used JC-1 probes to assess mitochondrial membrane potential, and observed that in the Blank group, there was a significant increase in JC-1 monomers, which showed green fluorescence, indicating a marked decrease in mitochondrial membrane potential. Conversely, in the treatment groups, mitochondrial membrane potential was significantly improved, with IL-6 ECM@GelMA demonstrating superior capacity to restore mitochondrial membrane potential (Fig. 6E and F) [45]. As mitochondrial dysfunction and membrane damage can lead to the accumulation of reactive oxygen species (ROS), which exacerbates mitochondrial dysfunction, we used the DCFH-DA probe to measure ROS levels in macrophages. The results showed a significant increase in ROS levels in the LPS-stimulated group, while the hydrogels were able to inhibit ROS accumulation, likely through the restoration of mitochondrial function (Fig. 6C and D) [46]. Additionally, ATP assays confirmed that compared to the Blank group, the ECM-loaded hydrogel groups effectively promoted mitochondrial function recovery (Fig. 6G).

In summary, these results further demonstrate that both types of hydrogels significantly improve damaged mitochondrial function, with IL-6-ECM@GelMA showing the most effective results.

3.8. In vivo OA model treatment effects

Osteoarthritis (OA) is a complex disease involving multiple cell types and mechanisms. In vitro experiments have demonstrated that ECM@GelMA and IL-6-ECM@GelMA hydrogels can inhibit M1 macrophage polarization and modulate the inflammatory microenvironment. However, the in vivo situation is more complex, so we constructed a rat OA model using the DMM (Destabilization of the Medial Meniscus) surgical procedure, with a Sham group that did not undergo DMM surgery. Two weeks post-surgery, we administered different treatments, including PBS and the two types of hydrogels. One of the most significant radiological features of OA is the reduction in joint space width (JSW). After 8 weeks, we observed the JSW in rats using X-ray imaging. Compared to the Sham group, JSW was significantly reduced in the PBS, ECM@GelMA, and IL-6-ECM@GelMA groups, with the IL-6-ECM@GelMA group showing notable improvement over the PBS group. This indicates that IL-6-ECM@GelMA, as a functionalized ECM hydrogel, has a significant effect in ameliorating joint degeneration ($P < 0.05$) (Fig. 7B–E). In addition to radiological assessments, we performed histological analysis using Hematoxylin and Eosin (H&E) staining and Safranin O-fast green staining to evaluate cartilage changes. H&E staining revealed that cartilage in the PBS group exhibited signs of erosion, abnormal cells, and structural damage, while cartilage in the Sham group was smooth, with normal cells and clear structure. Both types of hydrogels significantly improved these OA symptoms, with IL-6-

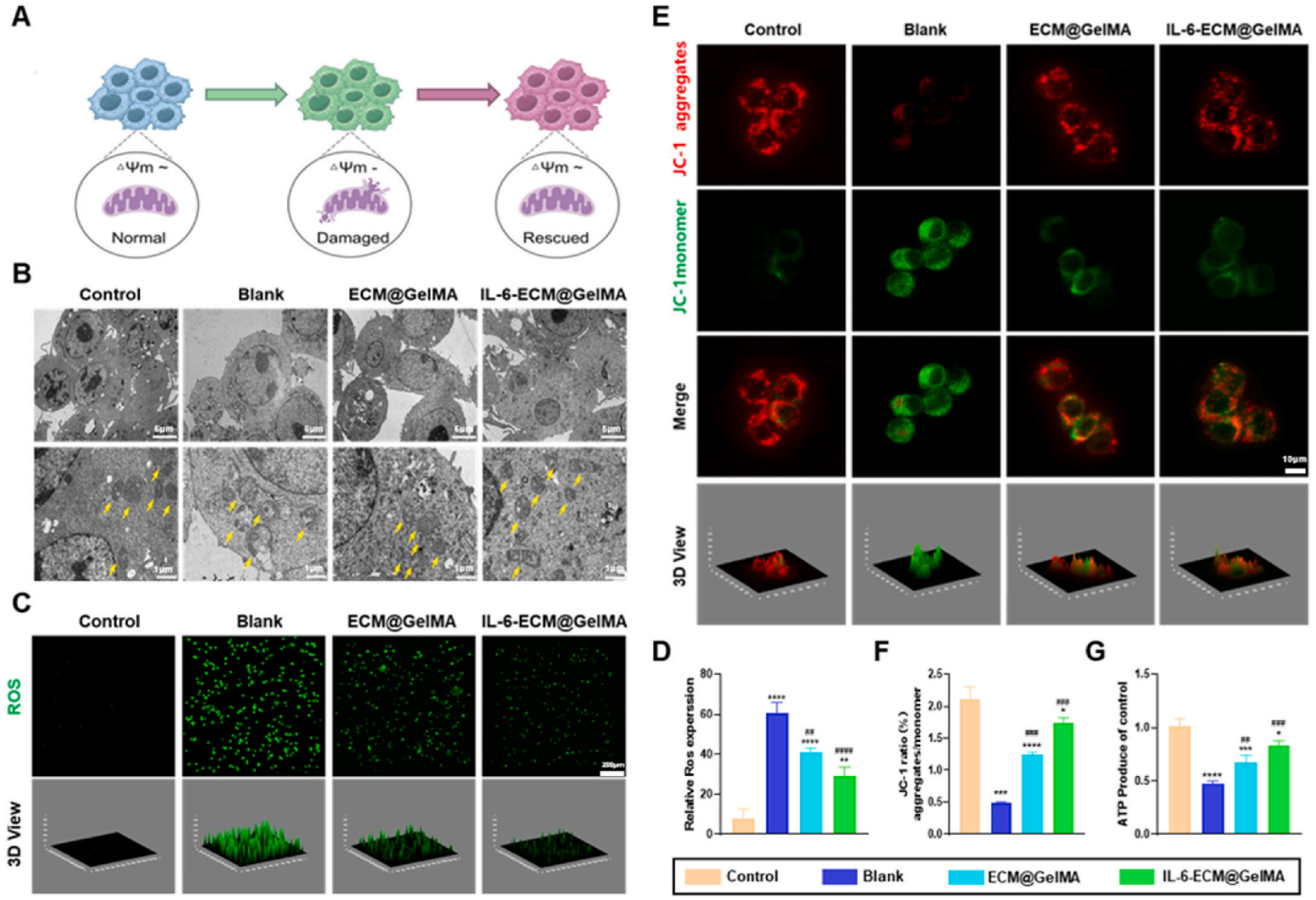

Fig. 6. Effect of ECM functionalized Hydrogel on Mitochondrial Function in Macrophages In Vitro: A. Schematic diagram showing how the hydrogel improves mitochondrial function. B. Transmission electron microscopy images of mitochondria in the control group, blank group, ECM@GelMA group, and IL-6-ECM@GelMA group. Arrows indicate mitochondria. C-D. Expression levels of ROS in macrophages from each group. E-F. Mitochondrial membrane potential levels in macrophages from each group. G. Expression levels of ATP in macrophages from each group. (Data are expressed as mean ± standard deviation, n = 3, */**/***/**** and#/##/###/#### indicated $p < 0.05/p < 0.01/p < 0.001/p < 0.0001$ in comparison with the Control and Blank groups, respectively).

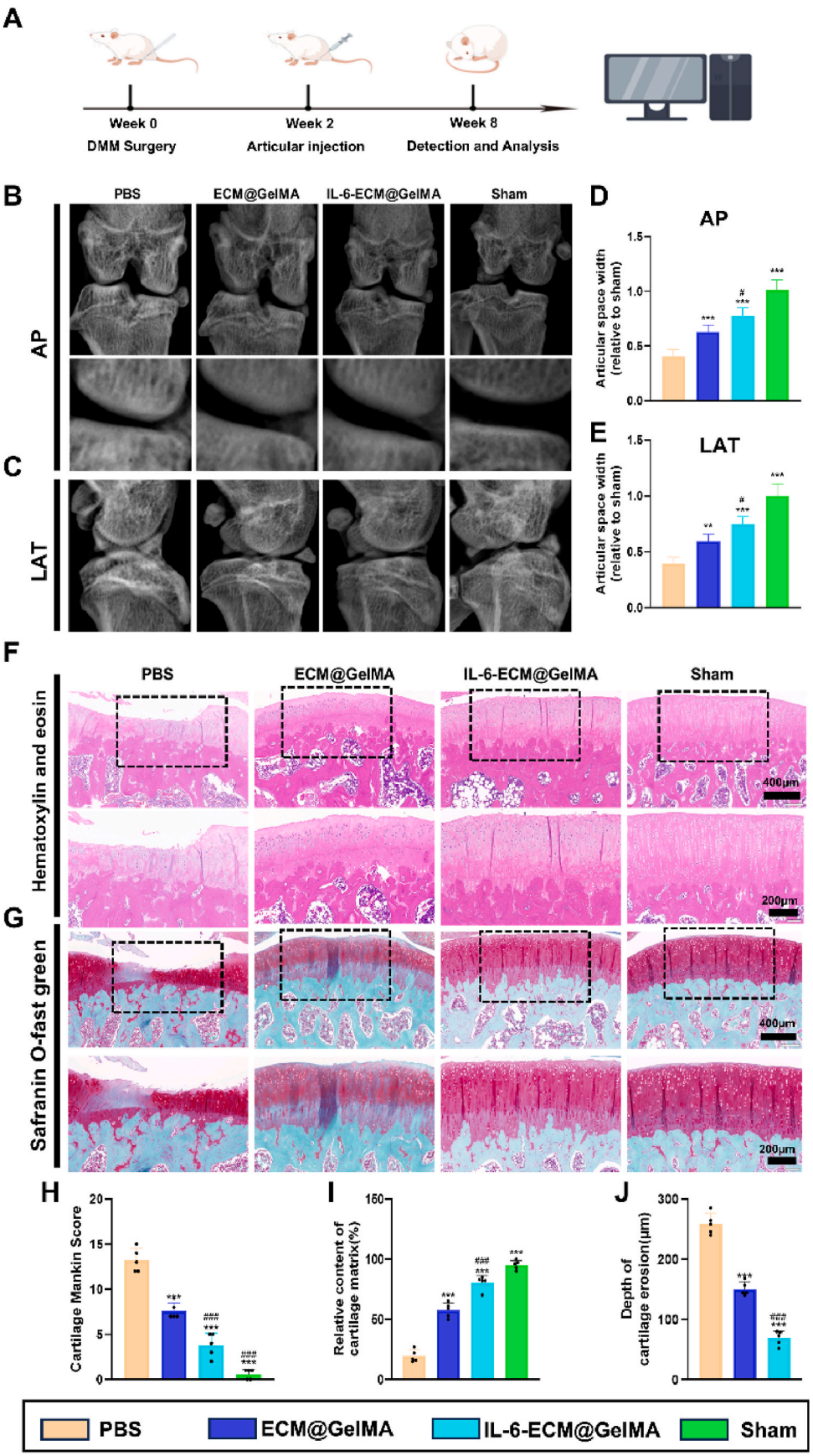

(caption on next page)

Fig. 7. X-ray and Histological Evaluation of Hydrogels for Treating Osteoarthritis in an SD Rat Model: A. Schematic diagram of animal modeling. B-C. Representative X-ray images of the knee joint in anteroposterior (AP) and lateral (LAT) views. D-E. Relative joint space width (JSW) measured from AP and LAT images. F. Representative H&E stained images of each group. G. Representative images of Safranin O-Fast Green staining of each group. H-J. Modified Mankin score, relative content of cartilage matrix, and cartilage erosion depth in each group. (Data are expressed as mean ± standard deviation, n = 5, */**/***/**** and#/##/###/#### indicated $p < 0.05/p < 0.01/p < 0.001/p < 0.0001$ in comparison with the PBS and ECM@GelMA groups, respectively).

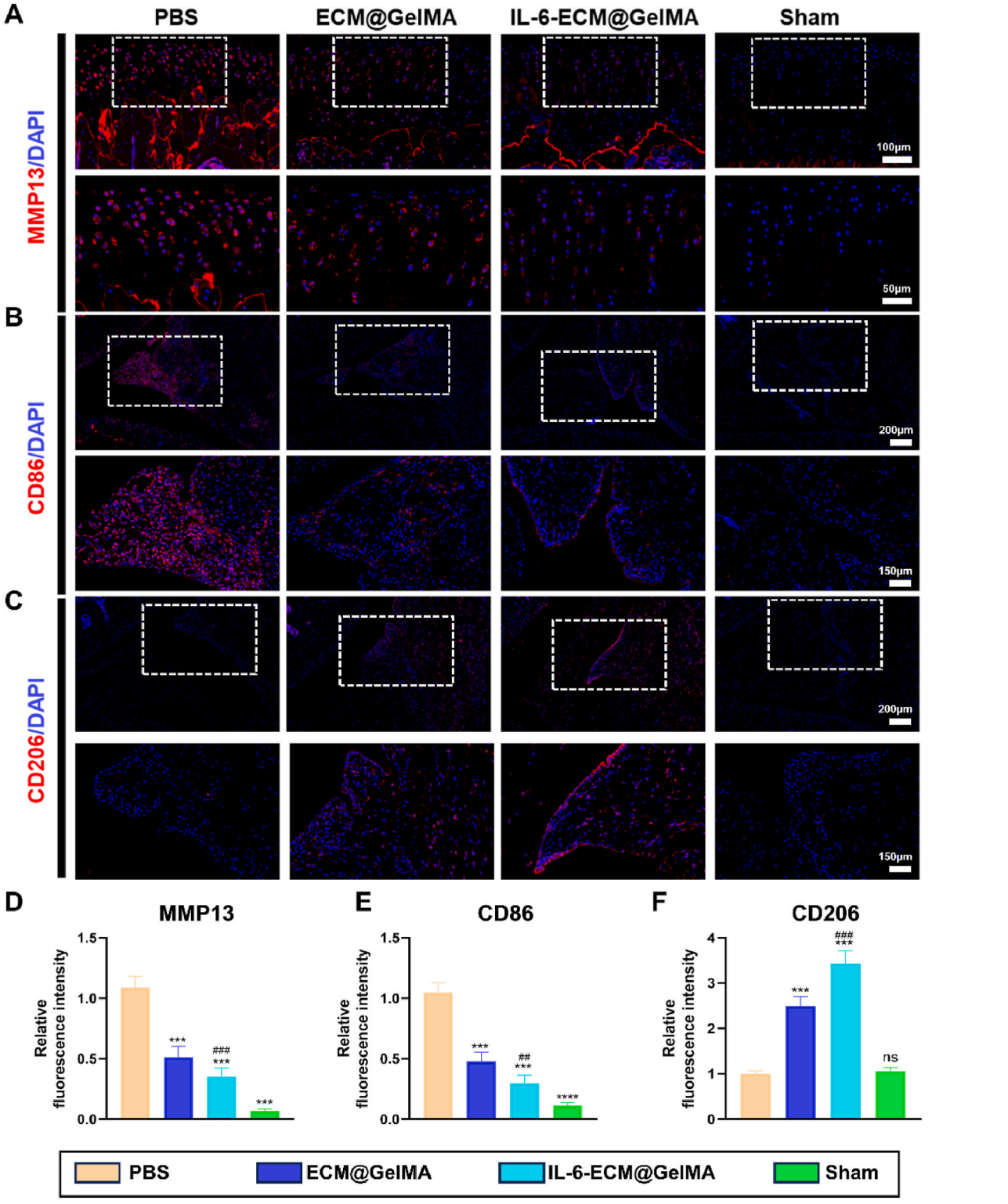

Fig. 8. Regulation of Macrophage Polarization by Hydrogel In Vivo: A-C. Immunofluorescence images of MMP13, CD86, and CD206. D-F. Quantification of immunofluorescence intensity for MMP13, CD86, and CD206. (Data are expressed as mean ± standard deviation, n = 5, */**/***/**** and#/##/###/#### indicated $p < 0.05/p < 0.01/p < 0.001/p < 0.0001$ in comparison with the PBS and ECM@GelMA groups, respectively).

ECM@GelMA demonstrating the most notable effect. Safranin O-fast green staining showed that collagen fibers were less stained in the OA rat group and somewhat reduced in ECM@GelMA, while IL-6-ECM@GelMA displayed minimal surface wear and no significant degeneration. Furthermore, the Mankin score for cartilage degeneration was significantly lower in the IL-6-ECM@GelMA group compared to the OA and ECM@GelMA groups. Analysis of cartilage matrix content and cartilage erosion depth also indicated that IL-6-ECM@GelMA effectively suppressed cartilage degeneration, outperforming ECM@GelMA ($P < 0.05$) (Fig. 7F–J) At the same time, we scored the synovial tissue, and the scoring criteria are shown in (Table S2). In the groups with ECM functionalized Hydrogel, synovial inflammation was significantly inhibited compared to the groups without ECM. (Fig. S4).

3.9. Regulation of the inflammatory microenvironment by hydrogels in vivo

In addition to cartilage degeneration, we also investigated whether the hydrogels could regulate macrophage polarization in vivo. To achieve this, we performed immunofluorescence staining on rat joint tissue sections. In the synovial tissue, where macrophages are predominantly located, we observed that CD86 expression was significantly increased in the PBS group, indicating a predominant M1 polarization state. However, treatment with the hydrogels effectively suppressed excessive M1 polarization and promoted M2 polarization, which is consistent with our in vitro findings ($P < 0.05$) (Fig. 8B–E). Additionally, MMP13 is an important protein involved in cartilage matrix degradation and serves as an indicator of joint inflammation. While MMP13 is expressed at low levels in healthy human joints, it is highly expressed in osteoarthritis patients. Our fluorescence results showed that IL-6-ECM@GelMA significantly inhibited MMP13 expression compared to PBS (Fig. 8A–F). This finding supports the notion that ECM hydrogels can exert anti-inflammatory effects through the modulation of macrophage polarization.

4. Conclusion

In summary, this study developed an ECM functionalized hydrogel loaded with IL-6 pre-stimulated ECM for the treatment of OA. Our in vitro experiments showed that this hydrogel has excellent biocompatibility, and IL-6-ECM@GelMA outperforms ECM@GelMA in enhancing mitochondrial function, metabolism, and regulating macrophage polarization. Subsequent in vivo experiments confirmed that IL-6-ECM@GelMA effectively regulates synovial macrophage metabolic reprogramming and reduces inflammation in the joint cavity. This novel ECM functionalized hydrogel represents a promising therapeutic approach to address the issue of macrophage polarization imbalance in OA.

CRediT authorship contribution statement

Zhuolin Chen: Writing – original draft, Validation, Methodology, Data curation, Conceptualization. **Qiming Pang:** Investigation, Formal analysis. **Jingdi Zhan:** Formal analysis. **Junyan Liu:** Formal analysis. **Weikang Zhao:** Supervision, Project administration, Methodology. **Lili Dong:** Project administration, Methodology, Conceptualization. **Wei Huang:** Writing – review & editing, Project administration, Formal analysis, Conceptualization.

Declaration of competing interest

The authors declare that they have no known competing financial interests or personal relationships that could have appeared to influence the work reported in this paper.

Acknowledgements

This work was sponsored by the National Natural Science Foundation of China-Joint Fund Project (U22A20284); Natural Science Foundation of Chongqing, China (CSTB2022NSCQ-BHX0683); Postdoctoral Special Funding Project of Chongqing Human Resources and Social Security Bureau (2112012726787861) and Postdoctoral Cultivating Project of the First Affiliated Hospital of Chongqing Medical University (CYYY-BSHPYXM-202202).

Appendix A. Supplementary data

Supplementary data to this article can be found online at https://doi.org/10.1016/j.mtbio.2024.101340.

Data availability

Data will be made available on request.

References

[1] Y. Jiang, Osteoarthritis year in review 2021: biology, Osteoarthritis Cartilage 30 (2) (2022) 207–215.
[2] C.T. Appleton, Osteoarthritis year in review 2017: biology, Osteoarthritis Cartilage 26 (3) (2018) 296–303.
[3] L. Qin, J. Yang, X. Su, L. Xilan, Y. Lei, L. Dong, H. Chen, C. Chen, C. Zhao, H. Zhang, J. Deng, N. Hu, W. Huang, The miR-21-5p enriched in the apoptotic bodies of M2 macrophage-derived extracellular vesicles alleviates osteoarthritis by changing macrophage phenotype, Genes Dis 10 (3) (2023) 1114–1129.
[4] N. Hannemann, F. Apparailly, G. Courties, Synovial macrophages: from ordinary eaters to extraordinary multitaskers, Trends Immunol. 42 (5) (2021) 368–371.
[5] T.A. Wynn, A. Chawla, J.W. Pollard, Macrophage biology in development, homeostasis and disease, Nature 496 (7446) (2013) 445–455.
[6] L. Zhang, X. Chen, P. Cai, H. Sun, S. Shen, B. Guo, Q. Jiang, Reprogramming mitochondrial metabolism in synovial macrophages of early osteoarthritis by a camouflaged meta-defensome, Adv. Mater. 34 (30) (2022) e2202715.
[7] A. Mathiessen, P.G. Conaghan, Synovitis in osteoarthritis: current understanding with therapeutic implications, Arthritis Res. Ther. 19 (1) (2017) 18.
[8] M.H.J. van den Bosch, Osteoarthritis year in review 2020: biology, Osteoarthritis Cartilage 29 (2) (2021) 143–150.
[9] K. Zhao, J. Ruan, L. Nie, X. Ye, J. Li, Effects of synovial macrophages in osteoarthritis, Front. Immunol. 14 (2023) 1164137.
[10] R.M. Samsonraj, M. Raghunath, V. Nurcombe, J.H. Hui, A.J. van Wijnen, S. M. Cool, Concise review: multifaceted characterization of human mesenchymal stem cells for use in regenerative medicine, Stem Cells Transl Med 6 (12) (2017) 2173–2185.
[11] M. Najar, H. Fahmi, Of mesenchymal stem/stromal cells and osteoarthritis: time to merge the latest breakthroughs, Stem Cell Rev Rep 16 (5) (2020) 1016–1018.
[12] D. Lu, X. Jiao, W. Jiang, L. Yang, Q. Gong, X. Wang, M. Wei, S. Gong, Mesenchymal stem cells influence monocyte/macrophage phenotype: regulatory mode and potential clinical applications, Biomed. Pharmacother. 165 (2023) 115042.
[13] H. Munir, H.M. McGettrick, Mesenchymal stem cell therapy for autoimmune disease: risks and rewards, Stem Cell. Dev. 24 (18) (2015) 2091–2100.
[14] J.L. Spees, R.H. Lee, C.A. Gregory, Mechanisms of mesenchymal stem/stromal cell function, Stem Cell Res. Ther. 7 (1) (2016) 125.
[15] F.J. Vizoso, N. Eiro, S. Cid, J. Schneider, R. Perez-Fernandez, Mesenchymal stem cell secretome: toward cell-free therapeutic strategies in regenerative medicine, Int. J. Mol. Sci. 18 (9) (2017).
[16] A. Gonzalez-Pujana, M. Igartua, E. Santos-Vizcaino, R.M. Hernandez, Mesenchymal stromal cell based therapies for the treatment of immune disorders: recent milestones and future challenges, Expet Opin. Drug Deliv. 17 (2) (2020) 189–200.
[17] J.M. Aamodt, D.W. Grainger, Extracellular matrix-based biomaterial scaffolds and the host response, Biomaterials 86 (2016) 68–82.
[18] X. Zhang, X. Chen, H. Hong, R. Hu, J. Liu, C. Liu, Decellularized extracellular matrix scaffolds: recent trends and emerging strategies in tissue engineering, Bioact. Mater. 10 (2022) 15–31.
[19] M. Brown, J. Li, C. Moraes, M. Tabrizian, N.Y.K. Li-Jessen, Decellularized extracellular matrix: new promising and challenging biomaterials for regenerative medicine, Biomaterials 289 (2022) 121786.
[20] L. Dong, L. Li, Y. Song, Y. Fang, J. Liu, P. Chen, S. Wang, C. Wang, T. Xia, W. Liu, L. Yang, MSC-derived immunomodulatory extracellular matrix functionalized electrospun fibers for mitigating foreign-body reaction and tendon adhesion, Acta Biomater. 133 (2021) 280–296.
[21] Y. Yu, H. Cui, C. Zhang, D. Zhang, J. Yin, G. Wen, Y. Chai, Human nail bed extracellular matrix facilitates bone regeneration via macrophage polarization mediated by the JAK2/STAT3 pathway, J. Mater. Chem. B 8 (18) (2020) 4067–4079.
[22] Y. Yu, H. Xiao, G. Tang, H. Wang, J. Shen, Y. Sun, S. Wang, W. Kong, Y. Chai, X. Liu, X. Wang, G. Wen, Biomimetic hydrogel derived from decellularized dermal matrix facilitates skin wounds healing, Mater Today Bio 21 (2023) 100725.

[23] M. Assunção, D. Dehghan-Baniani, C.H.K. Yiu, T. Später, S. Beyer, A. Blocki, Cell-derived extracellular matrix for tissue engineering and regenerative medicine, Front. Bioeng. Biotechnol. 8 (2020) 602009.
[24] C. Antich, G. Jiménez, J. de Vicente, E. López-Ruiz, C. Chocarro-Wrona, C. Griñán-Lisón, E. Carrillo, E. Montañez, J.A. Marchal, Development of a biomimetic hydrogel based on predifferentiated mesenchymal stem-cell-derived ECM for cartilage tissue engineering, Adv. Healthcare Mater. 10 (8) (2021) e2001847.
[25] S. Sart, R. Jeske, X. Chen, T. Ma, Y. Li, Engineering stem cell-derived extracellular matrices: decellularization, characterization, and biological function, Tissue Eng Part B Rev 26 (5) (2020) 402–422.
[26] J.R. Ferreira, G.Q. Teixeira, S.G. Santos, M.A. Barbosa, G. Almeida-Porada, R. M. Gonçalves, Mesenchymal stromal cell secretome: influencing therapeutic potential by cellular pre-conditioning, Front. Immunol. 9 (2018) 2837.
[27] V. Miceli, M. Bulati, G. Iannolo, G. Zito, A. Gallo, P.G. Conaldi, Therapeutic properties of mesenchymal stromal/stem cells: the need of cell priming for cell-free therapies in regenerative medicine, Int. J. Mol. Sci. 22 (2) (2021).
[28] S. Liu, S. Cheng, B. Chen, P. Xiao, J. Zhan, J. Liu, Z. Chen, J. Liu, T. Zhang, Y. Lei, W. Huang, Microvesicles-hydrogel breaks the cycle of cellular senescence by improving mitochondrial function to treat osteoarthritis, J. Nanobiotechnol. 21 (1) (2023) 429.
[29] M.J. Lee, J. Kim, M.Y. Kim, Y.S. Bae, S.H. Ryu, T.G. Lee, J.H. Kim, Proteomic analysis of tumor necrosis factor-alpha-induced secretome of human adipose tissue-derived mesenchymal stem cells, J. Proteome Res. 9 (4) (2010) 1754–1762.
[30] R. Nishimura, K. Hata, F. Ikeda, F. Ichida, A. Shimoyama, T. Matsubara, M. Wada, K. Amano, T. Yoneda, Signal transduction and transcriptional regulation during mesenchymal cell differentiation, J. Bone Miner. Metabol. 26 (3) (2008) 203–212.
[31] Z. Mima, K. Wang, M. Liang, Y. Wang, C. Liu, X. Wei, F. Luo, P. Nie, X. Chen, Y. Xu, Q. Ma, Blockade of JAK2 retards cartilage degeneration and IL-6-induced pain amplification in osteoarthritis, Int. Immunopharm. 113 (Pt A) (2022) 109340.
[32] M. Kapoor, J. Martel-Pelletier, D. Lajeunesse, J.P. Pelletier, H. Fahmi, Role of proinflammatory cytokines in the pathophysiology of osteoarthritis, Nat. Rev. Rheumatol. 7 (1) (2011) 33–42.
[33] A. Eitner, C. König, F.C. Kohler, G.O. Hofmann, B. Wildemann, M. Aurich, H. G. Schaible, Importance of IL-6 trans-signaling and high autocrine IL-6 production in human osteoarthritic chondrocyte metabolism, Osteoarthritis Cartilage 32 (5) (2024) 561–573.
[34] L. Edgar, A. Altamimi, M. García Sánchez, R. Tamburrinia, A. Asthana, C. Gazia, G. Orlando, Utility of extracellular matrix powders in tissue engineering, Organogenesis 14 (4) (2018) 172–186.
[35] H. Cao, L. Duan, Y. Zhang, J. Cao, K. Zhang, Current hydrogel advances in physicochemical and biological response-driven biomedical application diversity, Signal Transduct. Targeted Ther. 6 (1) (2021) 426.
[36] H. Lu, T. Hoshiba, N. Kawazoe, I. Koda, M. Song, G. Chen, Cultured cell-derived extracellular matrix scaffolds for tissue engineering, Biomaterials 32 (36) (2011) 9658–9666.
[37] E. Sanchez-Lopez, R. Coras, A. Torres, N.E. Lane, M. Guma, Synovial inflammation in osteoarthritis progression, Nat. Rev. Rheumatol. 18 (5) (2022) 258–275.
[38] W.H. Robinson, C.M. Lepus, Q. Wang, H. Raghu, R. Mao, T.M. Lindstrom, J. Sokolove, Low-grade inflammation as a key mediator of the pathogenesis of osteoarthritis, Nat. Rev. Rheumatol. 12 (10) (2016) 580–592.
[39] J. Van den Bossche, J. Baardman, N.A. Otto, S. van der Velden, A.E. Neele, S. M. van den Berg, R. Luque-Martin, H.J. Chen, M.C. Boshuizen, M. Ahmed, M. A. Hoeksema, A.F. de Vos, M.P. de Winther, Mitochondrial dysfunction prevents repolarization of inflammatory macrophages, Cell Rep. 17 (3) (2016) 684–696.
[40] J. Van den Bossche, L.A. O'Neill, D. Menon, Macrophage immunometabolism: where are we (going)? Trends Immunol. 38 (6) (2017) 395–406.
[41] R. Orihuela, C.A. McPherson, G.J. Harry, Microglial M1/M2 polarization and metabolic states, Br. J. Pharmacol. 173 (4) (2016) 649–665.
[42] X. Zheng, Y. Liu, Y. Liu, J. Zang, K. Wang, Z. Yang, N. Chen, J. Sun, L. Huang, Y. Li, L. Xue, H. Zhi, X. Zhang, M. Yu, S. Chen, H. Dong, Y. Li, Arginine-assembly as NO nano-donor prevents the negative feedback of macrophage repolarization by mitochondrial dysfunction for cancer immunotherapy, Biomaterials 306 (2024) 122474.
[43] P. Xiao, X. Han, Y. Huang, J. Yang, L. Chen, Z. Cai, N. Hu, W. Cui, W. Huang, Reprogramming macrophages via immune cell mobilized hydrogel microspheres for osteoarthritis treatments, Bioact. Mater. 32 (2024) 242–259.
[44] J. Faitg, T. Davey, D.M. Turnbull, K. White, A.E. Vincent, Mitochondrial morphology and function: two for the price of one!, J. Microsc. 278 (2) (2020) 89–106.
[45] A. Perelman, C. Wachtel, M. Cohen, S. Haupt, H. Shapiro, A. Tzur, JC-1: alternative excitation wavelengths facilitate mitochondrial membrane potential cytometry, Cell Death Dis. 3 (11) (2012) e430.
[46] S. Kasai, S. Shimizu, Y. Tatara, J. Mimura, K. Itoh, Regulation of Nrf2 by mitochondrial reactive oxygen species in physiology and pathology, Biomolecules 10 (2) (2020).